Thermal and Fluid Processes of a Thin Melt Zone during Femtosecond Laser Ablation of Glass

Adela Ben-Yakar[*a], Anthony Harkin[c], Jacqueline Ashmore[c], Mengyan Shen[b], Eric Mazur[b], Robert L. Byer[a], and Howard A. Stone[c]

a Applied Physics Department, Ginzton Laboratory, Stanford University, CA, USA 94305
b Department of Physics and Division of Engineering and Applied Sciences, Harvard University, Cambridge, MA, USA 02138
c Division of Engineering and Applied Sciences, Harvard University, Cambridge, MA, USA 02138

ABSTRACT

Microfluidic channels on borosilicate glass are machined using femtosecond lasers. The morphology of the ablated surface is studied using scanning microscopy. The results show micron scale features inside the channels. The formation mechanism of these features is investigated by additional experiments accompanied by a theoretical analysis of the thermal and fluid processes involved in the ultrafast laser ablation process. These studies indicate the existence of a very thin melting zone on glass and suggest that the surface morphology is formed by the plasma pressure-driven fluid motion of the melting zone during the ablation process.

Keywords: Femtosecond, laser, ablation, microfabrication, rim, glass, borosilicate, thin film, microchannels, microfluidics

1. INTRODUCTION

Microchannels fabricated on glass have a growing importance in the miniaturization of microfluidic devices for chemical and biological micro-total-analysis systems[1-3]. In most cases, the chips are fabricated using traditional multilayer and multistep photolithographic techniques. On the other hand, laser micromachining using ultrafast pulses offers a single-step method for direct writing of microchannels on glass. Using this laser ablation technique the fabrication speed can considerably be increased and geometries with variable depth and high-aspect ratio not possible through traditional microlithographic techniques can easily be achieved.

However, detailed morphology studies[4] of the laser-machined microchannels have demonstrated that micron-size features were formed inside the channels and the walls of the ablated surfaces were not smooth. It is necessary to investigate the formation mechanism of these small surface features to control and understand the micro-machining process using ultrafast lasers. We have performed a theoretical analysis of the thermal and fluid processes involved in the ultrafast laser ablation to explain and understand the experimental observations.

2. EXPERIMENTAL RESULTS

We carried out the experiments on borosilicate glass (Borofloat™ 1.1 mm thick, Precision Glass and Optics, Ltd.). The substrates were cleaned ultrasonically with alcohol before the experiments. After the ablation, the debris was removed with a 0.5 Molar sodium hydroxide (NaOH) solution (a very weak etching for about 20 minutes) followed by an alcohol rinse in the ultrasonic bath.

[*] adela@stanford.edu; phone: +1 (650) 723-0161; fax: +1 (650) 723-2666

Photon Processing in Microelectronics and Photonics II, A. Piqué, K. Sugioka, P. R. Herman, J. Fieret, F. G. Bachmann, J. J. Dubowski, W. Hoving, K. Washio, D. B. Geohegan, F. Träger, K. Murakami, Editors, Proceedings of SPIE Vol. 4977 (2003) © 2003 SPIE · 0277-786X/03/$15.00

The glass samples were irradiated with 800-nm 100-200-fs pulses from a regeneratively amplified Ti:sapphire laser with the surface of the sample positioned to be normal to the direction of the incident beam. Following irradiation, the samples were analyzed with a scanning electron microscope (SEM). The laser beam was delivered to the surface by a long working distance objective lens (Mitutoya, 5x, NA=0.14) attached to a microscope. On the surface of the target, the focused beam had a Gaussian spatial beam profile with a $1/e^2$ radius of $w_0 = 5.9$ μm[4]. The experiments were performed in a vacuum chamber at pressures below 10^{-4} mbar. A continuous channel was formed by moving the sample with a scanning speed of $v_{SS} = 1.5$ mm/s at 1 kHz laser repetition rate. The average number of pulses overlapping at the same spot was $N_{eff} = 6$. The resulting channel has a width of 9.6-μm and a depth of 2.5-μm. Figure 1 shows a typical surface morphology of a microchannel produced with 200-fs pulses at an average laser fluence (energy per unit area) of 12 J/cm^2. The most pronounced feature of the microchannel surface morphology (Fig. 1) is related to its non-smooth walls that have a surface roughness of the order of 1-μm.

An important clue explaining the mechanism of the microfeature formation could be determined from how the glass surface responds to a single laser pulse irradiation. Figure 2 presents SEM images of a crater generated with a single 100-fs laser pulse. The center of the crater demonstrates a smooth surface profile, whereas around the crater a 50-nm tall rim is raised above the surface. A detailed visualization of the elevated rim is shown in Figs. 2b and 2c. The observations suggest that the rim is a resolidified splash of a molten layer generated during the ablation process. In ultrafast laser ablation, the rapid energy deposition to the material allows material removal before significant heating of the bulk material occurs. Still, enough energy is deposited in the undamaged part of the material to create a shallow molten zone below the ablated area. We discuss the level of the material heating and estimate the melt depth. We present characteristic time scales of various mechanisms causing the melt to flow outwards to create the rim and show representative numerical simulations of fluid flow in a thin molten layer.

3. THEORETICAL MODELING AND DISCUSSION

A theoretical model is described to characterize the detailed thermal and flow processes associated with the first laser pulse. The goal is to identify the nature of the rim formation around the laser ablated craters and suggest ways (such as modification of the laser profile) to eliminate it. To estimate the melt thickness, optical light penetration and heat conduction into the material were taken into account. A thin film model is then proposed to predict the temporal evolution of the melt surface. The amount of the melt flow to the crater edge depends on the viscosity, the thickness of the molten layer, and the pressure distribution above the surface.

3.1. Heat transfer calculations

Absorbed laser energy and its partition

To calculate the thickness of the molten layer, the partition sequence of the absorbed laser energy must be determined. Specifically, we need to know what fraction of the laser energy remains in the bulk of the material and how this energy dissipates from the illuminated regime.

Vidal et al.[5] modeled the fluid and thermal dynamics of a laser-induced plasma for an aluminum target ablated with a 100-ps laser pulse. Their numerical simulation results provide the partition of the absorbed laser energy as a function of time. Typically after a few microseconds they found that most absorbed laser energy is used to move the ambient gas (~ 70%). A significant fraction of the absorbed energy (~ 20%) is lost in radiation and a small fraction (~ 10%) of the absorbed energy remains in the target as thermal energy.

However, to estimate the partition of the absorbed laser energy in the case of femtosecond laser ablation of glass, a further complicated numerical solution is required. We propose to use an effective optical light penetration depth to estimate the fraction of the incoming laser energy which remains in the glass as the thermal energy.

Optical light penetration depth

The volume/depth, where the laser energy is deposited initially, can be calculated using the effective absorption coefficient of the material. According to the Beer-Lambert law, which provides a convenient means to quantify the penetration depth of the absorbed laser energy, light attenuates with depth z according to

$$F_a(z) = A F_0^{avg} \exp\left(-\alpha_{eff} \cdot z\right) \tag{1}$$

where A is the surface absorptivity, α_{eff} is the effective material absorption coefficient (α_{eff}^{-1} is the effective optical penetration depth), F_0^{avg} is the average laser fluence (energy per unit area), and F_a is the laser fluence absorbed by the material.

Absorptivity of fused silica when exposed to high intensity ultrashort pulses, has been numerically calculated and experimentally measured by Perry et al.[6] They have demonstrated that when the incident intensity is high above threshold, a large portion of the energy can be reflected back into the ambient gas (due to the formation of a critical plasma density early in the pulse or in other words due to the induced skin effect). The reflectance of a fused silica surface using 10^{14} W/cm^2 of laser irradiance is estimated to be around 70%. Since a similar laser irradiance level is used in the current experiments, we can assume that only 30% of the incident beam gets absorbed by glass $(A = 0.3)$.

The value of the effective optical penetration depth, α_{eff}^{-1}, for borosilicate glass can be taken from our previous studies[4]. The ablation threshold measurements yield a linear relationship between the ablation depth, h_a, and the laser fluence according to

$$h_a = \alpha_{eff}^{-1} \ln\left(\frac{F_0^{avg}}{F_{th}^{avg}}\right) \tag{2}$$

where F_0^{avg} is the average fluence of the incident beam and F_{th}^{avg} is the average ablation threshold fluence ($F_{th}^{avg} = 1.7$ J/cm^2 for borosilicate glass)[4]. The slope of the linear fit to the experimental data points provides an optical penetration depth of $\alpha_{eff}^{-1} = 224$ nm for borosilicate glass (780-nm and 200-fs laser pulses in the fluence range of $F_0^{avg} = 10 - 30$ J/cm^2).

We may assume that the absorbed laser energy that penetrates beyond the measured ablation depth remains in the material as heat. Since the laser fluence at the ablation depth is equal to $F_a(z = h_a) = A F_{th}^{avg}$, the value of the thermalized energy remaining in the material as heat is

$$E_{heat} = A F_{th}^{avg} \cdot \pi w_0^2, \tag{3}$$

where w_0 is the $1/e^2$ laser beam radius at the surface. Thus a fixed amount of laser fluence about $A F_{th}^{avg} = 0.5$ J/cm^2 will be heating the undamaged part of the material independent of the incident laser fluence in the range of $F_0^{avg} = 10 - 30$ J/cm^2. At near threshold fluences, a larger amount of energy is expected to heat the material beyond the ablation depth as the surface absorptivity increases at lower fluences[6].

Melt depth

The ultrafast laser ablation process can be separated in two independent processes: absorption of the incoming light and dissipation of the heat. Initially electrons in the conduction band are excited with the absorbed laser energy. Only after the laser pulse is gone, energy is transferred from the high energy electrons to the lattice. Within a few picoseconds the excited electrons equilibrate with the ions (lattice) before any significant energy is dissipated by the heat diffusion into the material. The resulting initial equilibrium temperature (T_{eq}) can then be calculated according to the optical penetration depth of the laser light;

$$T_{eq}(z) = \frac{F_a(z)}{\rho C} = \frac{AF_0^{avg}}{\rho C \cdot \alpha_{eff}^{-1}} \exp\left(-\frac{z}{\alpha_{eff}^{-1}}\right) \tag{4}$$

assuming a constant heat capacity C. Melting occurs in a volume of heated material when the temperature exceeds the melting temperature (T_m). The glass transition temperature is used here as the melting temperature. Also note that the glass materials do not have a latent heat of melting. So, all the absorbed energy goes into melting.

Figure 3 shows a schematic illustration of the incident laser beam attenuation with depth and the resulting initial temperature distribution inside the glass material. When the material is illuminated with an ultrashort laser pulse, a high-temperature and high-pressure plasma is formed above the surface, presumably down to the ablation depth. The ablated material is removed by the expansion of the plasma. Below the plasma there is a thin zone of a molten glass with an initial thickness of $h_m(t=0) = 0.5$ μm, calculated using Eq. 4 (as the depth with temperature $T_{eq} > T_m$).

Following the cessation of ultrafast energy input, the melting process continues as the heat flows out of the initial light penetrated region. The speed at which the heat diffuses determines the melting front. Since the melting front moves with the heat source the heat penetration into the material will determine the variation of the melt thickness.

By taking AF_{th}^{avg} as the laser fluence that remains in the part of the material that is not ablated, the heat flow out of the regime can then be calculated by solving the one-dimensional (1-D) heat diffusion equation. The cooling at the top of the melt zone is assumed to be negligible because of the presence of the high temperature plasma. During the expansion, the plasma cools from some very high initial temperature to the ambient temperature which takes place in tens of microseconds.

Assuming the heat capacity, C, the thermal conductivity, k, and therefore the thermal diffusivity, $D = k/\rho C$ to be constant we can calculate the temperature distribution in the part of the material that is not ablated. Using the one-dimensional conduction model described by Nolte et al.[7] the equilibrium temperature as a function of $\tilde{z} = z - h_a$ is

$$T_{eq}(\tilde{z}) \cong \frac{AF_{th}^{avg}}{\rho C} \frac{1}{l^2 - \delta^2} \left[l \exp\left(-\frac{\tilde{z}}{l}\right) - \delta \exp\left(-\frac{\tilde{z}}{\delta}\right) \right] \tag{5}$$

where $l = \sqrt{D \cdot t}$ is the heat penetration depth and $\delta = \alpha_{eff}^{-1}$ is the optical penetration depth. Note that the temperature distribution at $t = 0$ is exactly the initial temperature distribution calculated previously according to the Beer-Lambert law. The variation of the melt depth can then be calculated as a function of time using Eq. 5.

Figure 4 presents a plot of melt depth variation with time for two different laser fluences thermalized in the material as heat; $F_{heat} = AF_{th}^{avg} = 0.5$ and $F_{heat} = AF_{th}^{avg} = 1.0$ J/cm^2. The melting process continues briefly for 1-3 μs and then solidification begins. These calculations provide us an estimate for the order of magnitude of two important characteristic scales of the melt zone:

1. Characteristic melt depth h_m (or h_0) of the order of 1 μm.
2. Characteristic melt life time τ_m of the order of 5-10 μs.

3.2. Fluid dynamics calculations

Thin film model

Here we treat a one-dimensional model of the fluid motion, which should be a good approximation since the molten layer has a depth much smaller than its radius. The free surface of the molten fluid is described by $z = h(x,t)$ and the lubrication approximation can be used to describe the fluid motion. The evolution equation is

$$h_t + \frac{\partial}{\partial x}\left(\frac{\gamma_x h^2}{2\mu} - \frac{dp}{dx}\frac{h^3}{3\mu}\right) = 0 \tag{6}$$

where μ is the viscosity, γ is the surface tension, and $p(x)$ is the time independent pressure of the plasma above the free surface. We have neglected the capillary contribution in the last term since this would only be important at late times when larger curvatures form. Also, because of the complicated dynamics of the plasma, for this initial modeling we assume that the plasma pressure field at the liquid surface is independent of time. When a temperature distribution, $T(x)$, is imposed along the surface, then

$$\gamma_x = \frac{d\gamma}{dx} = \frac{d\gamma}{dT}\frac{dT}{dx}. \tag{7}$$

If $\gamma_T = d\gamma/dT$ is constant and we neglect temperature effects on the viscosity, then we have

$$h_t + \underbrace{\frac{\gamma_T}{2\mu}\frac{\partial}{\partial x}\left(T_x h^2\right)}_{\text{Marangoni flow}} - \underbrace{\frac{1}{3\mu}\frac{\partial}{\partial x}\left(\frac{dp}{dx}h^3\right)}_{\text{pressure-driven flow}} = 0\,. \tag{8}$$

The first term accounts for the surface tension gradients (Marangoni flow) due to the uneven heating of the surface and the second term accounts for the motion due to the pressure gradients exerted by the plasma onto the molten material. Characteristic time scales associated with the Marangoni flow and the pressure-driven flow are

Marangoni flow: $$\tau_M \sim \frac{\mu L^2}{|\gamma_T| T_m h_0} \tag{9}$$

Pressure-driven flow: $$\tau_p \sim \frac{\mu L^2}{p_0 h_0^2} \tag{10}$$

where $|\gamma_T|$ is the absolute value of the temperature coefficient of surface tension, h_0 is an average melt depth, L is a typical radial dimension, and p_0 is an average plasma pressure. The values of material properties of borosilicate glass are summarized in Table 1. For an average melt depth of $h_0 \approx 1\,\mu\text{m}$ as estimated in the previous section and an average plasma pressure of $p_0 \sim 100$ atm (typical plasma pressure drops from millions of atmospheres to about ~20 atm during the first 200-ns of its expansion[8]) we obtain

$$\frac{\tau_M}{\tau_p} = \frac{|\gamma_T| T_m}{p_0 h_0} \approx 0.5\times 10^3\,. \tag{11}$$

The characteristic time scale for Marangoni flow is two to three orders of magnitude longer than the one for the pressure-driven flow. It is clear from this estimate that the plasma pressure above the free surface acts to move the fluid much more quickly than surface tension. This suggests that once an expanding plasma is formed above the glass surface during a laser ablation process of glass, the spatially varying plasma pressure will control the evolution of the free surface at the interface. In the context of laser texturing of silicon surfaces in the absence of ablation, however, the pump formation was attributed to the Marangoni flow in thin films created by nanosecond laser pulse heating[9].

Furthermore, the surface tension coefficient of borosilicate glass is positive in contrast to the normally observed negative values of most pure liquids. This means that the thermocapillary flow (Marangoni flow) in laser irradiated glass surfaces would actually drive fluid from the cold periphery to the hot center of the melt. Therefore, if the thermocapillary forces would act faster, a competition would have existed between the pressure gradients pushing on the surface and the thermocapillary forces.

After identifying that the effect of the thermocapillary flow is negligible during a laser ablation process, the surface evolution equation can be simplified to:

$$h_t - \frac{1}{3\mu}\frac{\partial}{\partial x}\left(\frac{dp}{dx}h^3\right) = 0\,. \tag{12}$$

If the bottom substrate of the molten fluid is not flat and given by $z = b(x,t)$ the evolution equation for the surface of the fluid becomes

$$h_t - \frac{1}{\mu}\frac{\partial}{\partial x}\left[\frac{dp}{dx}\frac{(h-b)^3}{3}\right] = 0\,. \tag{13}$$

Nondimensionalizing the time, length, height, and pressure by characteristic values

$$t \to \tau_p\, t', \qquad x \to Lx', \qquad h \to h_0 h', \qquad b \to h_0 b', \qquad p \to p_0 p' \tag{14}$$

leads to the following nondimensional equation

$$h_t' - \frac{\partial}{\partial x'}\left(\frac{dp'}{dx'}\frac{(h'-b')^3}{3}\right) = 0\,. \tag{15}$$

Numerical simulation results

Numerical calculations of Eq. 15 are performed on an unbounded domain for a pressure distribution given by $p = \exp\left(-x^{10}\right)$ which approximates closely a top hat profile that should be a reasonable approximation to the plasma pressure. The initial interface between the plasma and the melt is shaped and the molten layer has the same thickness as the ablation depth. The initial shape of the free surface initially is assumed to be $h(x) = 1 - 0.5\exp\left(-15x^{10}\right)$ and the shape of the bottom substrate is described by $b(x) = 0.9 - 0.8\exp\left(-x^{10}\right)$. The results, presented in Fig. 6, indicate that a rather tall rim (at the height of $0.25h_0 \approx 250$ nm) develops for a pressure-driven flow within a short time $t = 8$ μs (we have assumed $L = 10$ μm). There is a clear consistency between the rim formation time scale and the melt life time. This provides an indication that the rim is formed by the pressure gradient of the plasma within the life-time of the melt.

From the characteristic time scale, τ_p, (Eq. 10) one can identify the parameters that might effect the rim formation. One of the parameters is the melt thickness. A thinner melt zone will slow down the rim formation, and may even eliminate it.

4. CONCLUSIONS

The morphology of the single-shot ablated areas revealed a smooth and shallow crater surrounded by an elevated rim. From these experimental observations, conclusions could be drawn on the ablation mechanism of borosilicate glass. We argued that a very thin melt zone existed during the ablation process and calculated the thermal and flow properties of this thin melt zone. In these calculations, several characteristic time constants associated with ablation, melting, and flow processes were determined. The comparative values revealed that fluid would have enough time to move from the center of the melted region (the center of the crater) to the edge by way of a pressure-driven flow depositing a thin rim around the ablated area, where the origin of the pressure gradient is the high pressure above the surface.

ACKNOWLEDGEMENT

The work has been supported by the TRW research fund and the Harvard NSEC. The authors gratefully acknowledge the contributions of Dr. Catherine Crouch to this investigation.

REFERENCES

1. D. J. Beebe, G. A. Mensing, and G. M. Walker, "Physics and applications of microfluidics in biology." *Annu. Rev. Biomed. Eng.* **4**, p. 261-286, 2002.
2. J. Voldman, M. L. Gray, and M. A. Schmidt, "Microfabrication in biology and medicine." *Annu. Rev. Biomed. Eng.* 1, p. 401-425, 1999.
3. N. Giordano and J.-T. Cheng, "Microfluidic mechanics: progress and opportunities." *J. Phy.: Condens. Matter* **13** R271-R295
4. A. Ben-Yakar and R. L. Byer, "Femtosecond laser micromachining of microchannels on borosilicate glass." *Submitted for publication to J. of Appl. Phys.*, 2002.
5. F. Vidal, S. Laville, B. Le Drogoff, T. W. Johnston, M. Chaker,O. Barthélemy, J. Margot, M. Sabsabi, " Modeling of ablation plasmas for various laser pulse lengths." *From presentation in the Annual meeting of OSA*, Long Beach, CA, 2001.
6. M. D. Perry, B. C. Stuart, P. S. Banks, M. D. Feit, V. Yanovsky, and A. M. Rubenchik, "Ultrashort-pulse laser machining of dielectric materials." *J. of Appl. Phys.* **85** (9), p. 6803-6810, 1999.
7. S. Nolte, C. Momma, H. Jacobs, A. Tunnermann, B. N. Chichkov, B. Wellegehausen, and H. Welling, "Ablation of metals by ultrashort laser pulses." *J. Opt. Soc. Am. B* **14** (10), p. 2716-2722, 1997.
8. F. Vidal, S. Laville, T. W. Johnston, O. Barthelemy, M. Chaker, B. Le Drogoff, J. Margot, M. Sabsabi, "Numerical simulations of ultrashort laser pulse ablation and plasma expansion in an ambient air." *Spectrochimica Acta Part B*, **56**, p. 973-986, 2001.
9. T. Schwarz-Selinger, D. G. Cahill, S. C. Chen, S. J. Moon, and C. P. Grigoropoulos, "Micron-scale modifications of Si surface morphology by pulsed-laser texturing", *Physical Review B*, **64**, pp.155323, 1999.
10. W. D. Kingery, "Surface tension of some liquid oxides and their temperature coefficients", *J. Am. Cerm. Soc*., **42**, pp. 6-10, 1959.

Table 1: Properties of borosilicate glass (Borofloat©) with chemical composition of 81% SiO_2, 13% B_2O_3, 2% Al_2O_3, and 4% Na_2O.

Properties	**Symbol**	**Units**	**Values**
Density	ρ	kg/m^3	2.23×10^3
Melting temperature	T_m	K	1500
Viscosity	μ	Pa · s	$\approx 10^3$ at $T_m = 1500$ K $\approx 10^2$ at $T = 2000$ K
Surface tension	γ	J/m^2	0.28 [10]
Temperature coefficient of surface tension	$\partial\gamma/\partial T = \gamma_T$	N m^{-1} K^{-1}	$+3.4\times10^{-5}$ [10]
Thermal conductivity	k	W m^{-1} K^{-1}	1.25 (at 300 K) 1.6 (at 600 K)
Specific heat	C	J kg^{-1} K^{-1}	1000 (at 600 K)
Thermal diffusivity	$D = k/\rho C$	m s^{-2}	7.2×10^{-7} (at 600 K)

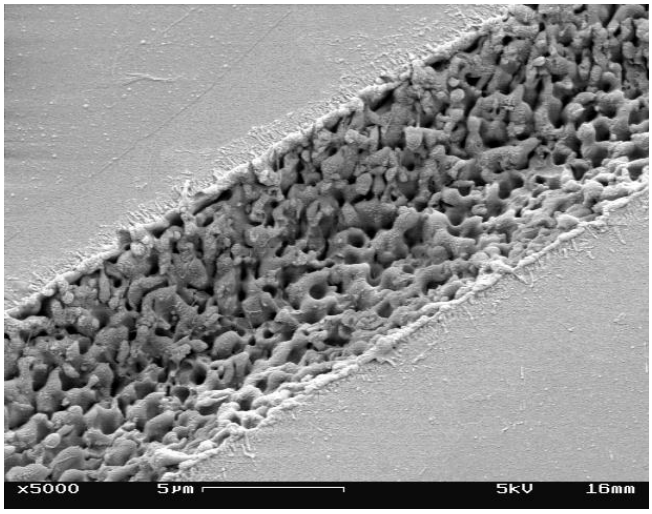

Figure 1: Surface morphology of a microchannel fabricated on borosilicate glass using 800-nm and 200-fs laser pulses. The channel is about 9.6-µm wide and about 2.5-µm deep. The effective number of overlapping pulses was about $N_{eff} = 6$ and the average laser fluence was 12 J/cm^2.

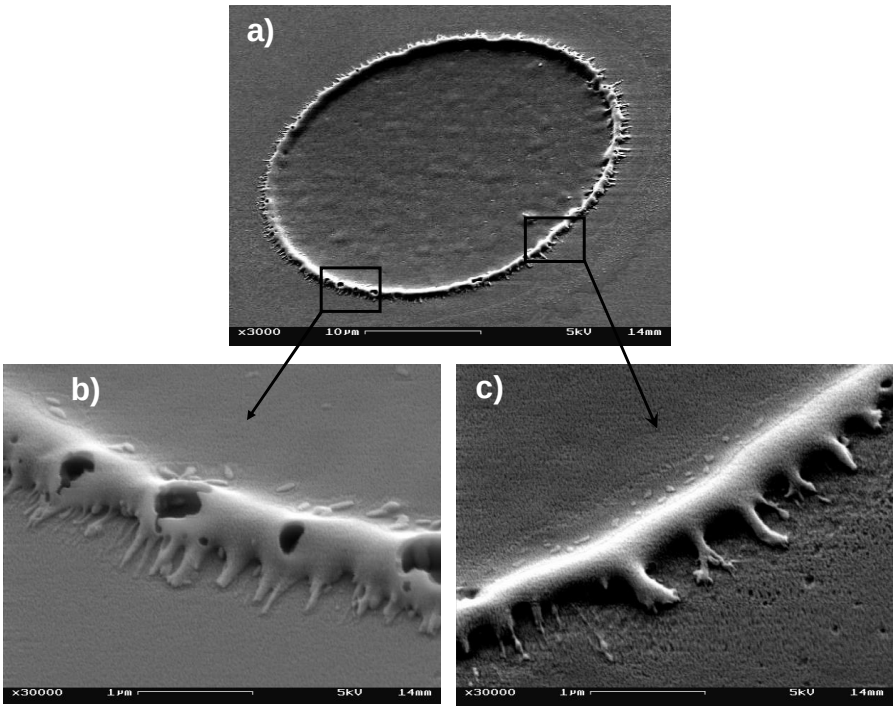

Figure 2: SEM images of a crater generated with a single laser pulse. (a) The whole crater at 3000× magnification and (b,c) two higher resolution SEM images (30,000× magnification) focused on the rim formed around the crater. The laser fluence was $F_0^{avg} = 34$ J/cm^2.

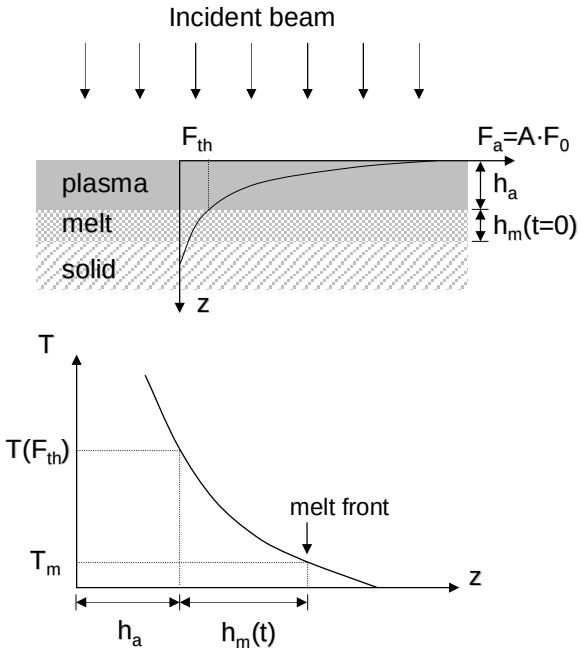

Figure 3: Laser absorption according to Beer-Lambert law and the resulting initial temperature distribution inside the material.

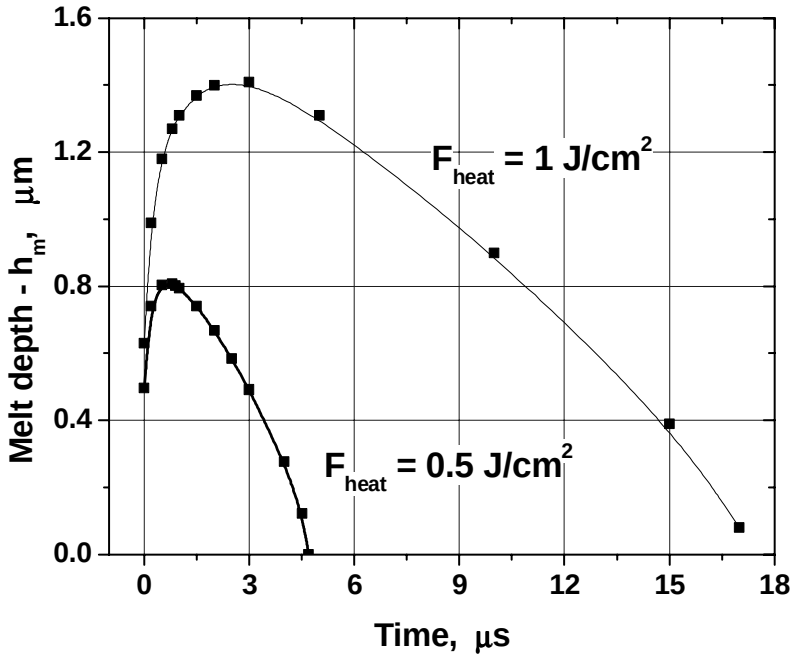

Figure 4: Calculated values of the melt depth variation with time for two different laser fluences that remain in the target (borosilicate glass) as thermal energy.

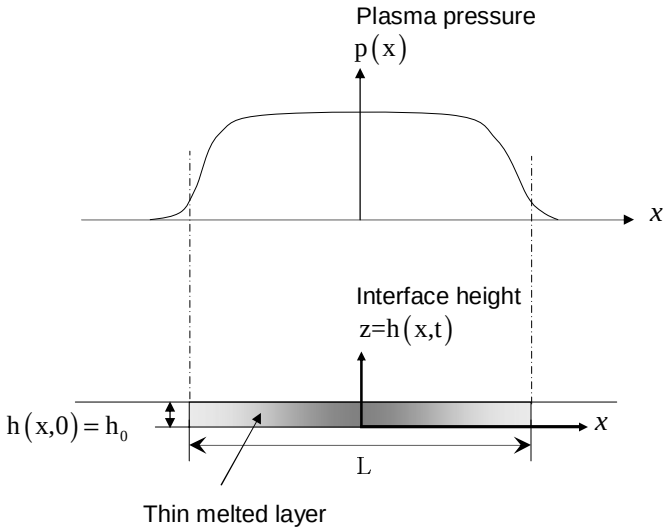

Figure 5. Description of parameters used in the thin film model to calculate the free melt surface evolution.

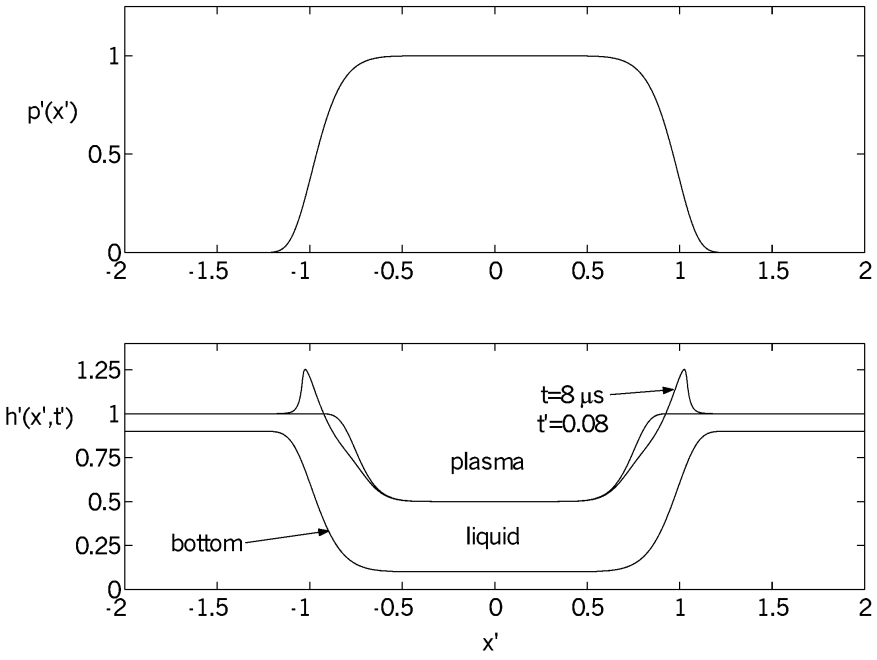

Figure 6. Numerical solution of pressure driven melt flow (Eq. 15) for a crater with a shaped bottom. The plasma pressure is shown in the top plot and is given by $p'(x') = \exp(-x'^{10})$. The bottom plot shows the evolution of the free surface at $t = 0$ and 8 μs. The crater is only half full of liquid (the rest got ablated).